

Article

Subsidence Management and Prediction System: A Case Study in Potash Mining

Nor Sidki-Rius *, Lluís Sanmiquel , Marc Bascompta  and David Parcerisa 

Department of Mining Engineering, Industrial and ICT, Polytechnic University of Catalonia (UPC),
Avenue Bases de Manresa, 61-73, 08242 Manresa, Spain

* Correspondence: nor.sidki@upc.edu

Abstract: Subsidence is an important environmental and safety issue in the mining sector, yet there remain voids in knowledge in terms of management and prediction. This study aims to improve knowledge on the impact of mining operations on the surface, reducing their effect on the environment, increasing the safety of mining operations, monitoring stress behavior and predicting rock mass. Therefore, an analysis was carried out to process and analyze the measured subsidence data and, subsequently, create a numerical model to predict the surface subsidence of a case study mine. The model was developed based on a finite element method (FEM). It was achieved by considering the geological characteristics of the area, the design features of the mine, the surface subsidence measured over twelve years and the time-dependent behavior of the geological layers. The correlation obtained between the measured subsidence and the modelling results was very satisfactory, with a 90% confidence level, over the years analyzed. Hence, the efficiency of the system was confirmed, enabling the evaluation and the prediction of potential surface effects, and therefore improving the safety and environmental levels of the mining area.

Keywords: subsidence; prediction; underground mining; finite element method (FEM); 2D modelling; geomechanics; environmental impact



Citation: Sidki-Rius, N.; Sanmiquel, L.; Bascompta, M.; Parcerisa, D. Subsidence Management and Prediction System: A Case Study in Potash Mining. *Minerals* **2022**, *12*, 1155. <https://doi.org/10.3390/min12091155>

Academic Editor: Abbas Taheri

Received: 15 July 2022

Accepted: 9 September 2022

Published: 13 September 2022

Publisher's Note: MDPI stays neutral with regard to jurisdictional claims in published maps and institutional affiliations.



Copyright: © 2022 by the authors. Licensee MDPI, Basel, Switzerland. This article is an open access article distributed under the terms and conditions of the Creative Commons Attribution (CC BY) license (<https://creativecommons.org/licenses/by/4.0/>).

1. Introduction

Mineral resources are crucial to providing welfare to society, so it is necessary to find and extract them on a sustainable basis. Nowadays, the mining industry represents a key factor in the development of societies and communities around ore deposits [1,2]. However, mining activity must be managed properly, since the effects of the extraction process can produce serious environmental problems in the vicinities of the mining area, such as acid drainage, heavy metal contamination of soils or subsidence [3,4]. In recent decades, various initiatives have emerged to construct the legal frameworks and legislate on the sustainability of extractive activities [5–7].

In the case of subsidence, it is well known that when mineral extraction is not properly planned, it has a high probability of having a direct impact on the surface, affecting not only mining infrastructures but also urban infrastructures or the communities that live close to the mining area [8–10]. In addition, subsidence has become of special importance as it is closely linked to the overexploitation of groundwaters [11–13]. Groundwaters represent one of the most important natural resources for ecosystems, as stated in the Sustainable Development Goals (SDGs) declared by the United Nations [14]. Various mining and geological factors, including the quality and characteristics of the underground rock and the surface conditions, can influence the subsidence magnitude, shape, mode, and extent [15]. Therefore, it is necessary to consider the usage of less aggressive mining methods as part of corporate social responsibility (CSR) [16].

The need for mineral resources pushes the industry towards extracting ores at greater depths, with buildings and infrastructures on the surface or with challenging bedrocks

such as soft or weak geological material [17–20]. Thus, long-time deformations related to underground excavations in areas with weak rocks still require further investigation [21–24]. One of the time-dependent mechanisms that weaken the rock is the creep phenomenon, commonly associated with evaporite or clay minerals [25–27]. Several studies have been performed to analyze this behavior by employing 3D modelling [28–31]. However, it can be complex and time-consuming to analyze different subsidence scenarios in a large mining area. Consequently, there is a need to investigate optimal numerical analyses to assess the geomechanical behavior in such scenarios. The option of two-dimensional modelling requires a method of “pseudo” time-dependent behavior, with two alternatives: (a) progressively relaxing the tunnel boundary tractions from a range of in situ stresses to zero at the last stage [32] or (b) modifying the geomechanical characteristics of the original materials [33].

Subsidence control and prediction have become very relevant in recent decades [34–36]. However, it is difficult to standardize a particular methodology, so it is more common to find approaches for each specific case [37]. Peng [38] defines six categories of subsidence prediction methods: theoretical, profile function, influence function, empirical, physical and numerical modelling. There are some advantages and disadvantages in each case [39]. Nevertheless, it is crucial to monitor and control subsidence evolution using actual data in order to calibrate and validate any chosen method [40]. Other examples of subsidence monitoring, control and prediction include interferometry synthetic aperture radar (InSAR) [41–43], analyzing subsidence by monitoring its spatio-temporal evolution [44–46]. The impact of subsidence has also been shown by several authors, assessing its environmental implications [47,48]. For example, Bell et al. [49] discuss the effect of subsidence on the environment in several cases to exemplify types of subsidence assimilated and related issues—for example, gold mines in the Johannesburg area, chalk and limestone mines in Suffolk and the West Midlands, and salt mines in Cheshire.

This study aims to obtain a method to manage subsidence data, using the global positioning system (GPS) and InSAR, and predict its potential effect through the numerical finite element method (FEM).

Case Study

This study was developed based on data from a mine located in northeastern Spain which extracts potash using a room and pillar method at depths between 500 and 700 m, varying the extraction rate depending on the arrangement of the stratum. The ore deposit is made of two different mineable layers, Bed A and Bed B, with an additional intermediate layer of varying thickness made of salt and clay minerals. Two different drifts are used to extract the potash ore when the salt layer is more than 5 m thick, while it is mined jointly when the thickness is less than 5 m. Bed A and Bed B are interstratified layers of sylvinite rock salt and clay minerals. The average production during the period 2007–2019 was 2,870,570 tons.

2. Materials and Methods

2.1. Data Management

The case study has approximately 700 control points in an area of 50 km², with measures taken from 2008 to 2021. These control points are distributed throughout the geographical area potentially affected by subsidence, obtaining the X, Y, and Z coordinates of each point using GPS. The post-process method is employed to obtain the coordinates, using four static differential GPS with double frequency receptors. Two receptors are placed at two points of known and well-established coordinates, while the other two receptors are used to perform measurements in the control points, with a minimum measurement time per point of 12 min. This methodology guarantees an accuracy of 1–1.5 cm in planimetric and altimetric coordinates, which implies that the maximum possible error between measures from the same point is 2–3 cm. Consequently, only higher differences are relevant to

indicate if there is subsidence. Regular quality control measurements are taken to verify the reliability of the measurements.

InSAR images are also used, since 2016, as an additional control system. Nonetheless, the surface characteristics of the area, mainly forested and agricultural, still require a considerable amount of GPS control points to obtain reliable subsidence displacement. In this case, it was determined that a minimum of 200 points are required. The accuracy of this type of technology was widely proved [50–52]. The combination of both systems allows for obtaining extremely reliable information regarding X, Y, and Z surface displacements [39].

2.2. Data Processing

The case study area is defined by the fully exploited zones from 2008 to 2018 based on the subsidence data collected. The initial year, 2008, is determined as it is the first year in which surface subsidence data are obtained. The final year, 2018, is determined according to Sanmiquel et al., 2018 [39], where it is stated that 90% of the surface subsidence for an active mine occurs within the initial 5 years.

Five profiles are defined within the area of interest. Each profile crosses the area completely, every 10 m in the direction of the mine advance, east–west, and Metric Points (MPs) are listed. These MPs show the displacement in the Z coordinate for each subsidence calculation period. According to Sanmiquel et al. [39], a 400-meter protection area is determined in order to separate the targeted area from the area exploited before 2008, as no data is available (Figure 1).

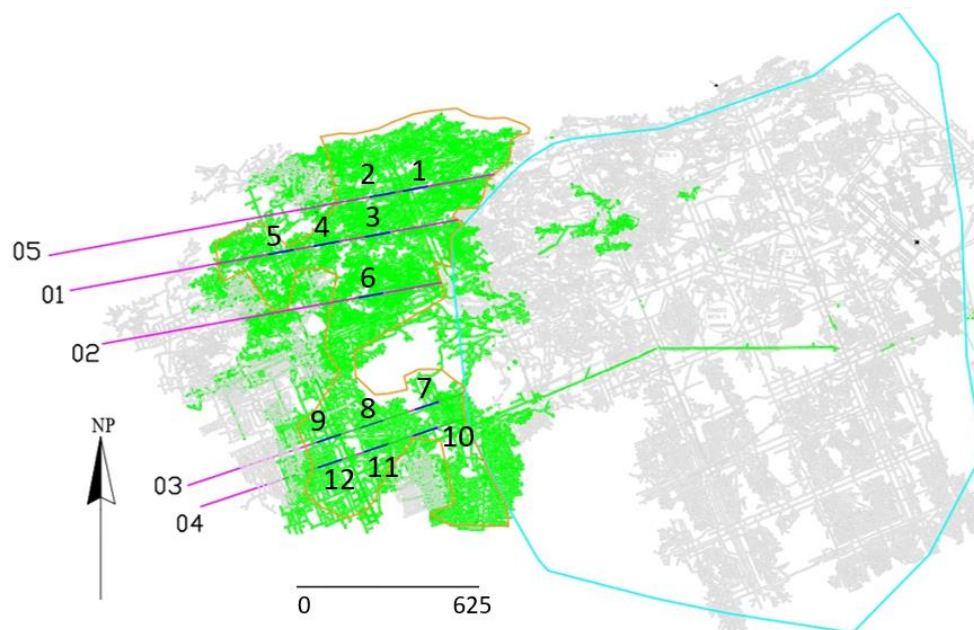


Figure 1. The mining area, with the two different perimeters, the five profiles and the twelve selected zones shown. The numbers on the left show the ID of each profile (from 01 to 05). The numbers enclosed in the orange perimeter show the ID of each analysed zone (01 to 12).

After analyzing all the raw data collected, the MPs are reduced and re-listed every 100 m, since it is considered an adequate distance to appreciate the evolution of subsidence. Figure 1 shows the targeted area in the enclosed orange perimeter and the mining drifts excavated during the years 2008–2018 are marked in light green. The light blue perimeter delimits the area exploited before 2008. Pink lines depict the 5 profiles used to determine the average subsidence of the targeted area, while dark blue marks the 12 mining zones selected to test the model, as they have been sorted from north to south and east to west, respectively. On the other hand, Figure 2 shows the targeted area amplified, so that the five profiles and the 12 selected mining zones can be seen in more detail as well as the 400-meter protection area.

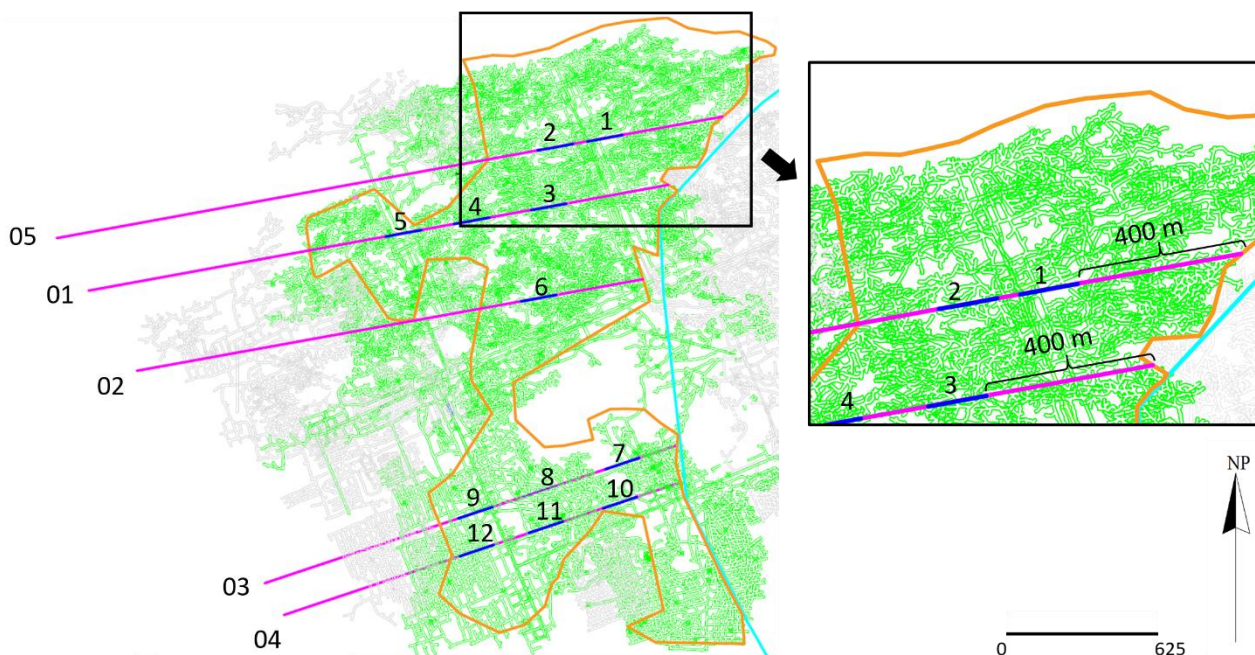


Figure 2. The targeted area used for the study and localization of the profiles.

The analysis is initially performed individually, defining how subsidence evolves over annual and biannual measurements. Subsequently, subsidence values are gathered together to obtain the profile of maximum subsidence for each MP and perform a statistical analysis to determine the average subsidence profile of the targeted area, as well as the level of confidence of the subsidence measured. Figure 3 represents the methodology to follow and obtain the average surface subsidence profile. The characteristics of the case study are in brackets.

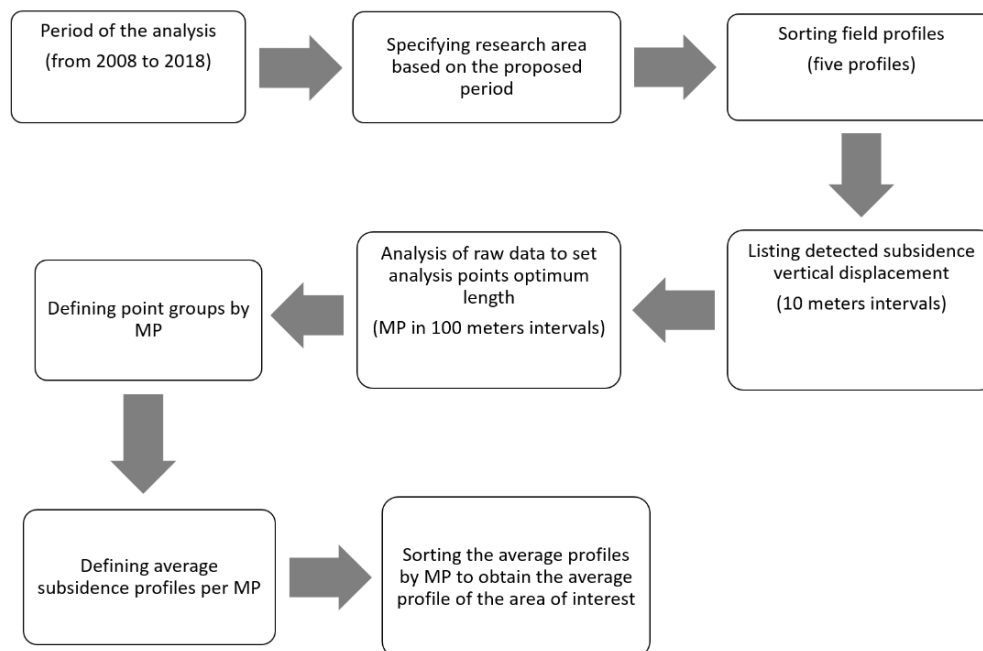


Figure 3. The methodology followed to reach the average surface subsidence profile.

2.3. Numerical Model Definition

The numerical model was generated using indirect time-dependent behavior modelling, using the RS2 v11.003 software (Toronto, ON, Canada). After analyzing the ge-

ometries of the drifts and the extraction ratio, an initial model was run. The total size of the model is 225 m by 666 m, with a minimum of 37.5 m of walls on each side; therefore, 150 m of exploitation is modelled. The model size is based on the stratigraphic column size proposed by Orellana et al., 1996 [53]. The models developed by Xu et al. [31] and Parmar et al. [30] have been used to define the wall width. The drifts are designed with an average geometry section, 6 m in height and 8.157 m in width, based on real mine planning. The mesh consists of 6 nodal triangles, while it is graded and densified around 150 m of the mined area, as well as in the areas of lithological variations to adequately capture displacements adjacent to the drift wall. No support material was placed in the drifts. The Mohr–Coulomb constitutive model was adopted for the analysis.

The model was designed based on the stratigraphic column taken from Campos de Orellana [53] and subsequently modified by Cendon et al. [54], adding two horizons of Anhydrite and Halite on top of those, known as roof salt. RS2 model is presented in Figure 4, where all the materials can be seen. The first lithology consists of sedimentary material such as sandstones, limestones and lutites, the second group of lithologies consists of two layers of anhydrite. These two groups of stratum correspond to the overburden part of the model. The following layers are defined by the potassic seams, formed by carnallite, Bed B, intermediate salt, Bed A, and footwall salt, and finally comes the last lithology formed by the lower salt. Figure 4 is not to scale, the top and bottom have been cut off, only showing the middle part of the model, which is considered the representative part of it. The geomechanical values of the lithologies were determined by laboratory and field testing, while some data were taken from Campos de Orellana [53]. Table 1 shows the values of geomechanical properties for each lithology.

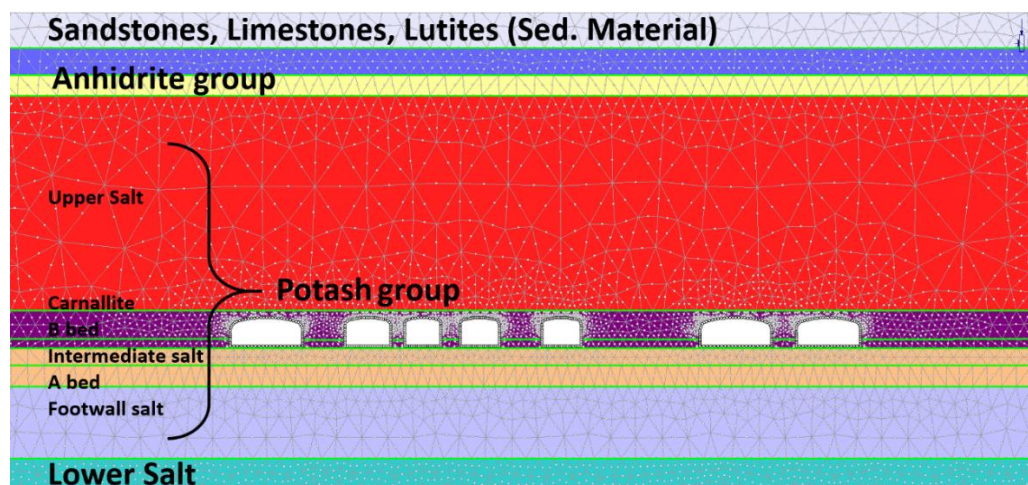


Figure 4. Example of an RS2 model with the geological and drifts characteristics.

Table 1. Values of geomechanical properties for each lithology.

Lithology	Sedimentary Material	Anhydrite Material 01	Anhydrite Material 02	Upper Salt	Potassic Layer 01	Potassic Layer 02	Footwall Salt	Lower Salt
Unit weight (kN/m ³)	26.55	29.7	23.5	23.7	19.8	21	21	21
Poisson ratio	0.31	0.3	0.26	0.29	0.145	0.215	0.2	0.2
Young's modulus (kPa)	3.57×10^7	4×10^7	3.09×10^6	5.3×10^6	5.19×10^6	2.19×10^6	1.38×10^6	1.38×10^6
Tensile strength (kPa)	4850	6040	2680	3900	2330	2650	2500	2500
Friction angle (degrees)	34	33	30	35	36	45	45	35
Cohesion (kPa)	6970	13,600	9755	3800	2100	3277.5	2900	2900

The materials with time-dependent behavior are the following lithologies: carnallite, Bed B, intermediate salt, Bed A and footwall salt. Seven stages have been defined, each one representing a two-year period. As can be seen in Figure 5, in the first stage, the original properties of the geological materials have been used, while Young’s modulus of the materials with time-dependent behavior was reduced from the second stage onwards. Figure 6 illustrates the methodology to define Young’s modulus decrease. The first modulus reduction was defined according to Paraskevopoulou et al. [21], while the following reductions are determined by an iterative approach (Figure 6), comparing the actual subsidence data and RS2 values.

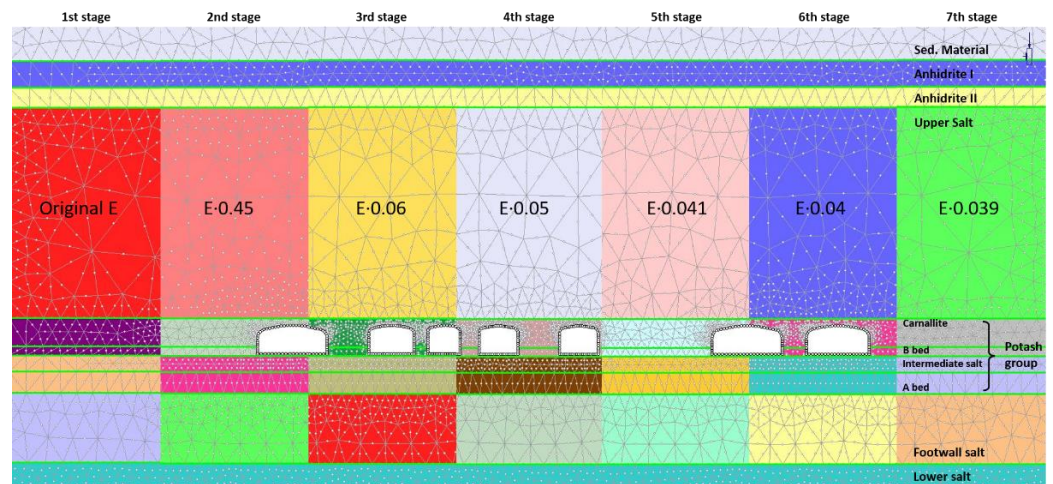


Figure 5. Example of the seven stages and their associated Young’s modulus (E).

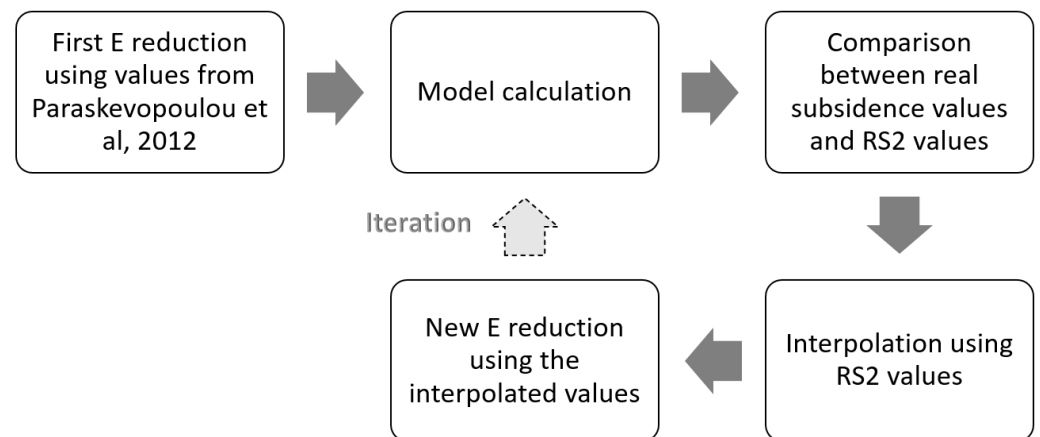


Figure 6. The methodology followed to define Young’s modulus decrease.

The factor used in each stage to reduce Young’s modulus is included in Figure 5, weakening the material properties of the model as a time-dependent behavior. The determination of the geomechanical characteristics of each stage is verified using the surface subsidence values. Once all the steps of the initial model were verified, it was tested in 12 selected mining zones, all of them included in the target area. The selection of these zones was performed randomly in order to achieve better representativity of the procedure proposed and its usage.

3. Results and Discussion

The technique to indirectly assess the time-dependent behavior allows for obtaining the following outcome. Results related to the definition of the average subsidence profile are presented, followed by the results obtained with RS2. Figures 7 and 8 show how subsidence evolves, at point MP 03 (which corresponds to the first 300 m), in the five profiles

tested between 2008 and 2021. The relative values are represented in Figure 7, showing the magnitude of surface subsidence year by year. On the other hand, Figure 8 displays the cumulative evolution of subsidence at point MP 03 during the period studied, obtaining a representation of the maximum values of subsidence and how surface subsidence evolves from year to year. In both figures, it can be observed how the maximum vertical displacement occurs during the years 2012 to 2016, with the period 2012–2014 the one with the steepest slope, hence the one with the maximum subsidence. This behavior is in accordance with previous studies performed in the area [39]. From 2016 onwards, it can be observed how the vertical subsidence is progressively reduced until it became stable during the period 2018–2021.

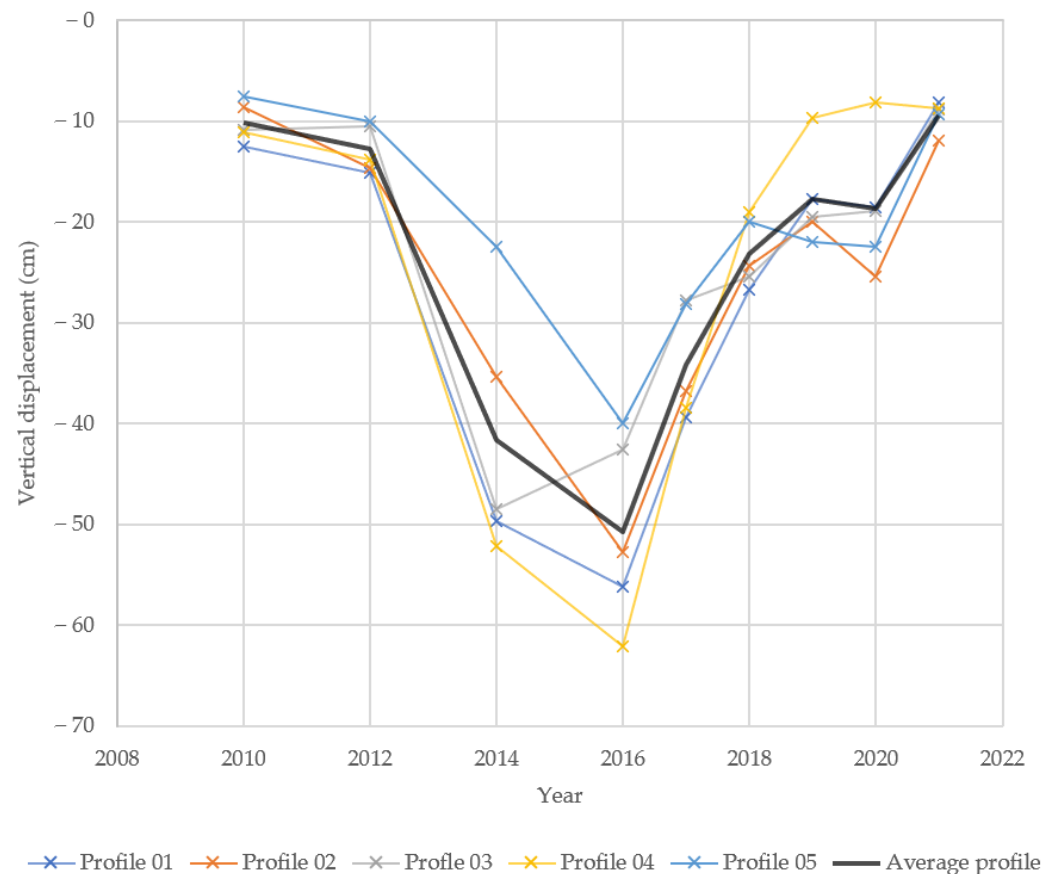


Figure 7. Relative subsidence values in MP 03.

Profile 4 shows the clearest subsidence evolution since it can be observed how the subsidence velocity evolves progressively in the first stages, increasing until reaching its maximum value of it in the period 2014–2016, followed by a reduction in the period 2016–2020, until reaching the stabilization of the subsidence velocity in the period 2020–2022. This subsidence trend is possible due to the fact that it is the profile located in the south part of the mine (Figure 1), being the least influenced by the whole group of mining drifts and excavations. Its analysis shows how the subsidence increases until reaching the maximum vertical displacement in 2016. From this date forward, vertical displacement is gradually reduced, reaching a stabilization stage during the period 2018–2021. On the other hand, the other profiles are located in areas where mining was more sustained in the period 2019–2020 and forward, making it more difficult to see the stabilization progress.

The average subsidence profile of the area of interest can be determined by means of the average subsidence profile from each MP. Figure 9 shows the average subsidence profile with a 90% confidence level. It can be seen that the maximum variability of the analyzed values is detected around the years 2016 and 2020 since these are the years in

which the raw subsidence data have the greatest variability. The data detailed in Figure 9, and processed, have been used to define the decreasing Young’s modulus (Figure 5). As can be seen in Figure 6, the reduction in Young’s modulus in each stage varies from that observed by Paraskevopoulou et al. [21], since it was adapted to the subsidence conditions of the case study. Nevertheless, the fundamental procedure applied remains the same.

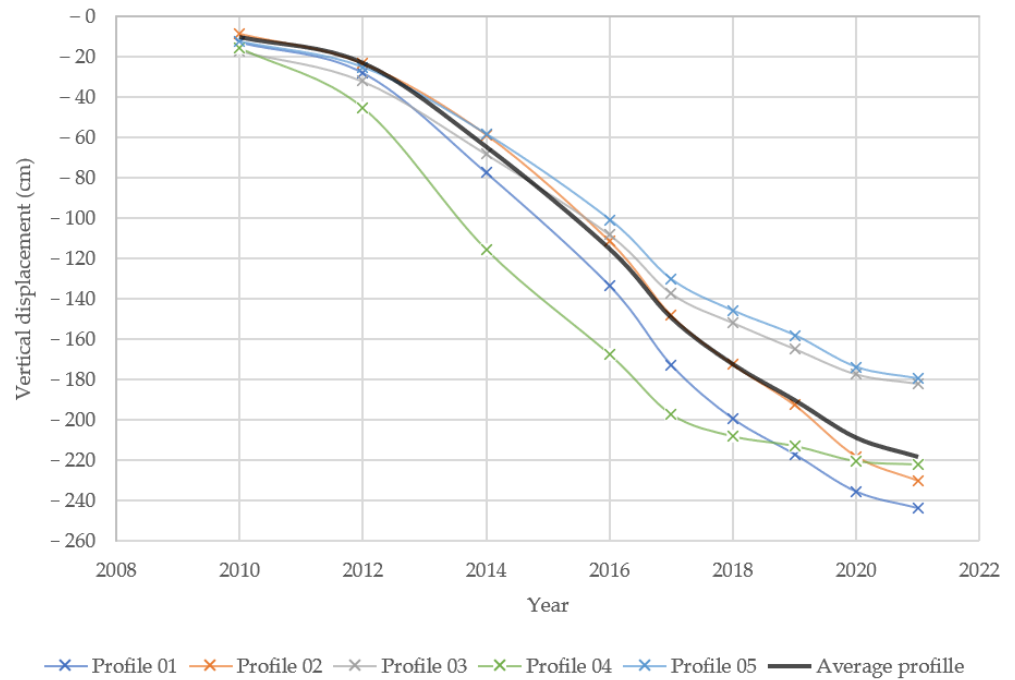


Figure 8. Maximum subsidence values of MP 03.

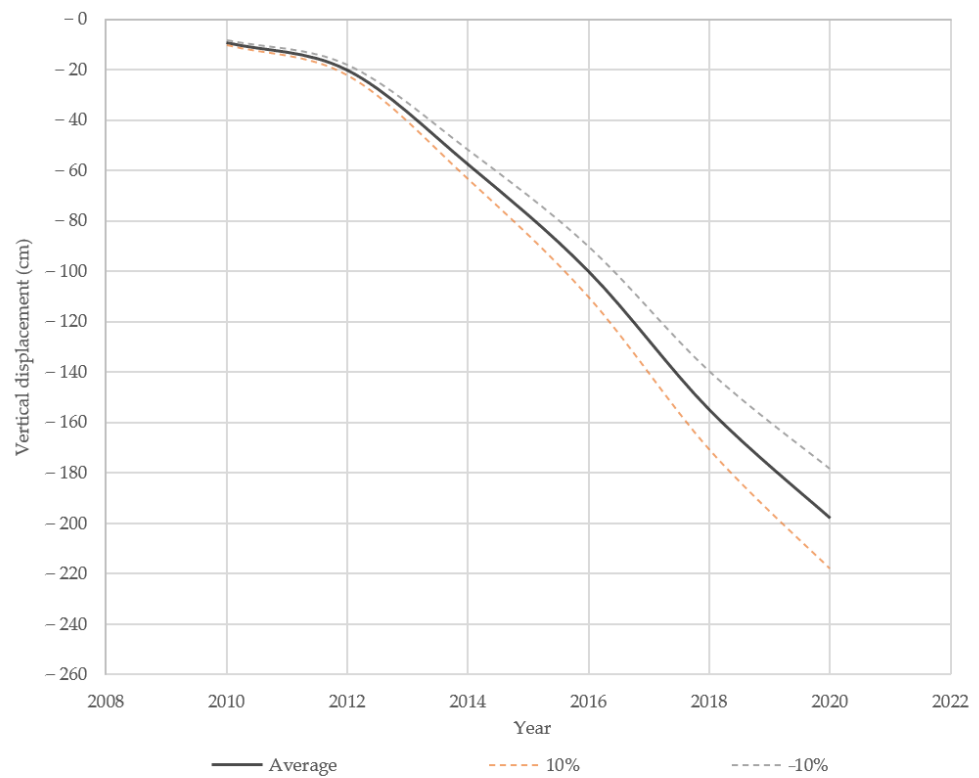


Figure 9. Average subsidence profile together with a 90% confidence level.

Surface subsidence values have been used to calibrate the FEM model by comparing them with vertical displacement values located on the surface of the model. Figure 10 shows one example of the stages obtained after the FEM post-process calculation, where it can be seen how the vertical displacement evolves throughout the stratigraphy that forms the ore deposit. These values, in all the evaluated mining areas, are homogeneously shown on the surface of the model, as can be seen in Figure 10. Yet, the actual subsidence values show variations in all the evaluated MPs. Thus, the average subsidence profile must be used to verify and calibrate the model (Figure 9). The model is proposed to enable the analysis of subsidence scenarios depending on the extraction ratio, depth and size of the drifts in a very user-friendly approach. The idea is that both the parameters to be introduced and those returned by the model are as simple as possible to be applied in the day-to-day life of a mining company, which represents the main advantage of the model. Therefore, the predicted values of the vertical surface displacements are considered average values. The model was tested in 12 different cases, and as a result, all tests were verified with real subsidence data.

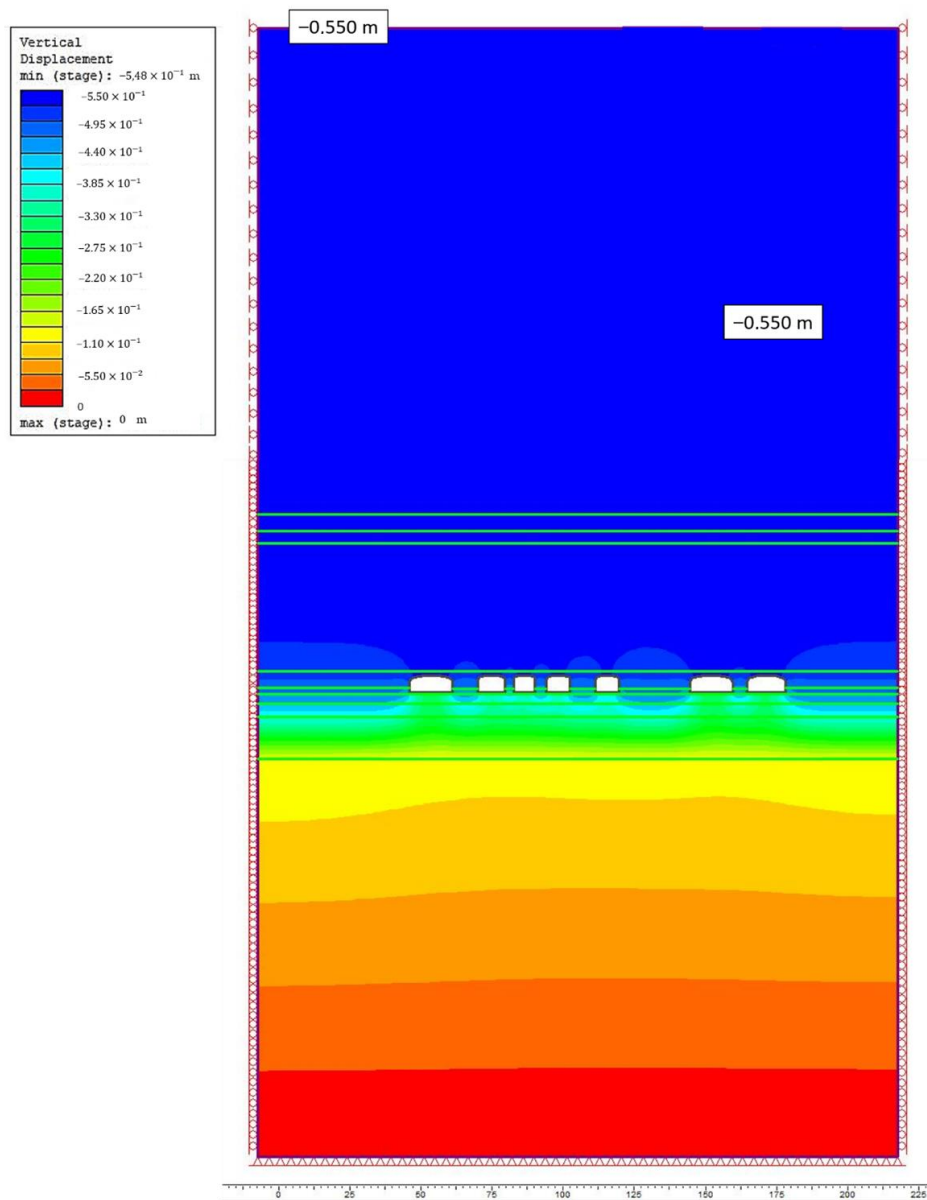


Figure 10. Example of the FEM post-processing stage achieved using RS2.

Table 2 shows the values obtained for the twelve mining zones tested, the average subsidence profile with a 90% level of confidence. It can be seen that in most of the stages, the values obtained with the RS2 model are within the level of confidence (Figure 11). In the first stage, the vertical displacement obtained by the FEM model ranges between −14.2 and −15.2 cm, being slightly out of the interval of −8.7 and −9.7 cm defined by the level of confidence of the actual values. This may be due to the values used as original material properties from laboratory tests could have some variation from their real in situ characteristics. However, the variation is still quite small and corrected over time with the subsidence evolution model. The main limitation is detected in the final stage, where subsidence stabilization should be modelled. However, achieving this trend requires recovering the initial properties in the last stage, which leads to an inconsistency with Young’s modulus reduction technique. Another disadvantage of the software used is the need to simplify the model design. Therefore, if much detail is required, this fact can represent a limitation. In the case of the twelve models tested, only the main geological structures were detailed.

Table 2. Average subsidence values with a 90% confidence level and values of the sections assessed.

Stage	Average Subsidence Value (cm)	+10% Error (cm)	−10% Error (cm)	Mining Zones Tested with RS2 Software (cm)											
				01	02	03	04	05	06	07	08	09	10	11	12
01	−9.197	−10.117	−8.277	−14.200	−15.000	−15.000	−15.200	−15.200	−15.000	−15.000	−15.000	−15.200	−15.200	−15.000	−15.200
02	−20.096	−22.106	−18.086	−19.000	−19.000	−20.000	−19.900	−21.000	−19.000	−19.000	−19.000	−20.900	−19.900	−19.000	−19.900
03	−57.531	−63.284	−51.778	−54.200	−54.000	−56.000	−60.000	−62.000	−55.000	−55.000	−56.000	−62.700	−59.000	−54.000	−59.000
04	−100.116	−110.128	−90.104	−99.000	−98.000	−99.000	−110.000	−114.000	−99.000	−100.000	−99.000	−117.000	−110.000	−98.000	−110.000
05	−155.067	−170.574	−139.560	−152.000	−150.000	−152.000	−162.000	−171.000	−152.000	−152.000	−152.000	−181.000	−162.000	−143.000	−162.000
06	−198.082	−217.890	−178.274	−200.000	−200.000	−200.000	−219.000	−228.000	−200.000	−200.000	−210.000	−238.000	−219.000	−200.000	−219.000
07	−209.125	−230.038	−188.213	−257.000	−247.000	−257.000	−276.000	−285.000	−260.000	−260.000	−260.000	−304.000	−280.000	−250.000	−276.000

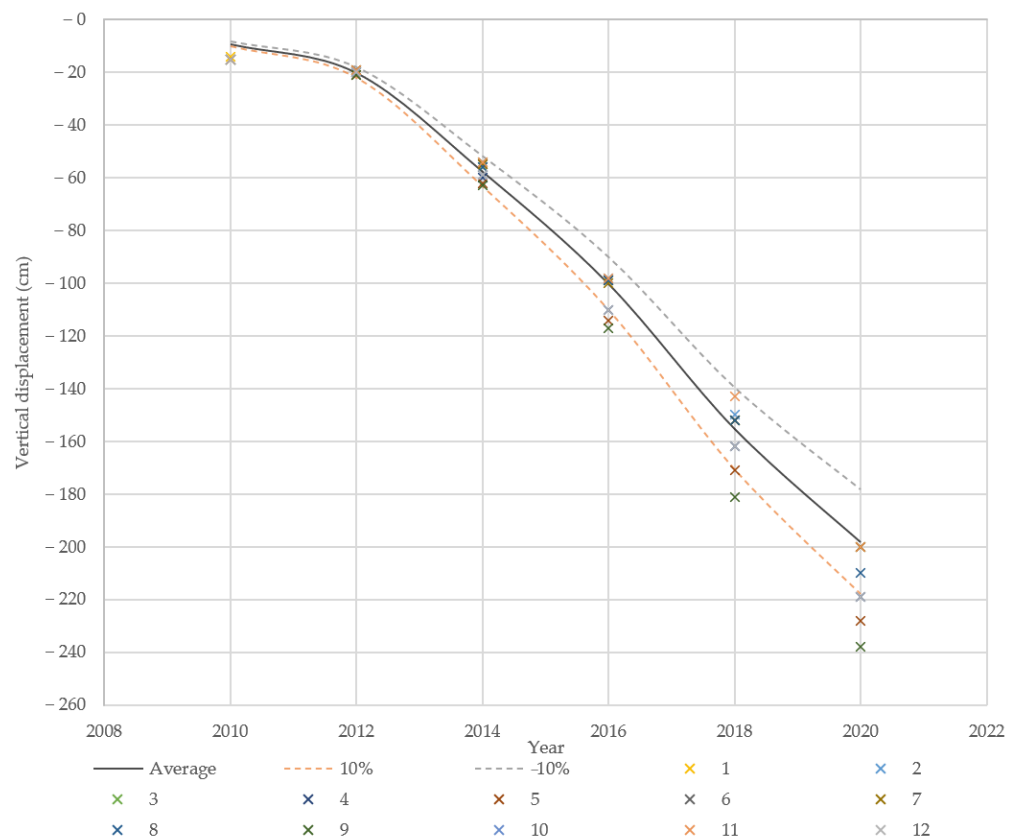


Figure 11. Average subsidence profile with the results of the sections analyzed.

Another factor to consider is the subsidence measured on the surface, using GPS. As mentioned in the methodology, it has a potential error between 2 and 3 cm. This means that the differences between real and theoretical values could be accepted when a range of ±5 cm is not exceeded and can, therefore, be considered accurate.

Based on the results from the numerical modeling, the 2D FEM method allows handling the nonlinear and inhomogeneous properties of rock masses that produce the time-dependent behavior. The model is a useful tool for the prediction of subsidence in mining infrastructures [30,31], as well as for analyzing and testing the time-dependent behavior [21]. It was detected that the most affected areas by subsidence are those with the widest mining galleries. This type of gallery is usually built when it is necessary to connect two parts of the mine infrastructure. In these cases, it is recommended to use underground supports and to have sufficiently wide pillars to limit their effect on the surface. In order to gain knowledge and improve the approach proposed, it would be interesting to test other areas, either potassic deposits or other rock types, with time-dependent behaviors.

4. Conclusions

The approach proposed gives the possibility to determine the evolution of subsidence over time. The system allows the generation of average profiles at different points and an average subsidence profile of an area. The system also provides crucial information on mining activity behavior and gives the possibility to analyze the subsidence velocity of a representative period in a very simple and straightforward way, which represents one of the major strengths of the assessed technique. The tested numerical method has sufficient capacity to evaluate the time-dependent behavior of the potash and salt layers, using an indirect method—a 2D FEM model.

Although the model has some limitations in achieving subsidence stabilization in the final stage, it was proven as a particularly useful tool, especially during the years of mining activity. The model is able to analyze potential extraction scenarios and measures taken to reduce the subsidence whenever it is necessary and, therefore, reduce the environmental impact of the mining extraction and increase the operational safety levels.

Author Contributions: Conceptualization, N.S.-R., L.S. and M.B.; methodology, N.S.-R., L.S. and M.B.; validation, N.S.-R., L.S., M.B. and D.P.; formal analysis, N.S.-R. and L.S.; investigation, N.S.-R., L.S., M.B. and D.P.; writing—original draft preparation, N.S.-R. and M.B.; writing—review and editing, N.S.-R., L.S., M.B. and D.P. All authors have read and agreed to the published version of the manuscript.

Funding: This research received no external funding.

Acknowledgments: The authors would like to thank ICL-Iberia for the data provided.

Conflicts of Interest: The authors declare no conflict of interest.

References

1. Vintró Sánchez, C.; Comajuncosa, J.M. Corporate social responsibility in the mining industry: Criteria and indicators. *Dyna* **2010**, *77*, 31–41.
2. Sanz, J.; Tomasa, O.; Jimenez-Franco, A.; Sidki-Rius, N. Elements and mineral resources. In *Nature*; Springer International Publishing AG: Cham, Switzerland, 2022.
3. Álvarez-Vigil, A.; González-Nicieza, C.; Gayarre, F.L.; Álvarez-Fernández, M. Forensic analysis of the evolution of damages to buildings constructed in a mining area (Part II). *Eng. Fail. Anal.* **2010**, *17*, 938–960. [[CrossRef](#)]
4. Gayarre, F.L.; Álvarez-Fernández, M.; González-Nicieza, C.; Álvarez-Vigil, A.; García, G.H. Forensic analysis of buildings affected by mining subsidence. *Eng. Fail. Anal.* **2010**, *17*, 270–285. [[CrossRef](#)]
5. Helm, P.; Davie, C.; Glendinning, S. Numerical modelling of shallow abandoned mine working subsidence affecting transport infrastructure. *Eng. Geol.* **2013**, *154*, 6–19. [[CrossRef](#)]
6. Kratzsch, H. *Mining Subsidence Engineering*; Springer Science & Business Media: Berlin/Heidelberg, Germany, 2012.
7. Virgone, K.M.; Ramirez-Andreotta, M.; Mainhagu, J.; Brusseau, M.L. Effective integrated frameworks for assessing mining sustainability. *Environ. Geochem. Health* **2018**, *40*, 2635–2655. [[CrossRef](#)]
8. Figueroa-Miranda, S.; Tuxpan-Vargas, J.; Ramos-Leal, J.A.; Hernández-Madrigal, V.M.; Villaseñor-Reyes, C.I. Land subsidence by groundwater over-exploitation from aquifers in tectonic valleys of Central Mexico: A review. *Eng. Geol.* **2018**, *246*, 91–106. [[CrossRef](#)]
9. Commission of the European Communities. *Promoting Sustainable Development in the EU Non-Energy Extractive Industry*; Office for Official Publications of the European Communities: Luxembourg, 2000.

10. Ford, C. Towards sustainable mining: The Canadian mining industry sustainability initiative. In *A Review on Indicators of Sustainability for the Minerals Extraction Industries*; Bôas, R.C.V., Shields, D.J., Šolar, S.V., Anciaux, P., Önal, G., Eds.; CYTED-CETEM: Rio de Janeiro, Brazil, 2004.
11. Nadiri, A.A.; Habibi, I.; Gharekhani, M.; Sadeghfam, S.; Barzegar, R.; Karimzadeh, S. Introducing dynamic land subsidence index based on the ALPRIFT framework using artificial intelligence techniques. *Earth Sci. Inform.* **2022**, *15*, 1007–1021. [[CrossRef](#)]
12. Nadiri, A.A.; Moazamnia, M.; Sadeghfam, S.; Barzegar, R. Mapping risk to land subsidence: Developing a two-level modeling strategy by combining multi-criteria decision-making and artificial intelligence techniques. *Water* **2021**, *13*, 2622. [[CrossRef](#)]
13. Gharekhani, M.; Nadiri, A.A.; Khatibi, R.; Sadeghfam, S. An investigation into time-variant subsidence potentials using inclusive multiple modelling strategies. *J. Environ. Manag.* **2021**, *294*, 112949. [[CrossRef](#)]
14. United Nations. *The Sustainable Development Goals Report*; United Nations: New York, NY, USA, 2022; ISBN 978-92-1-101448-8.
15. HUNTS. Surface Subsidence Due to Coal Mining in Illinois. Ph.D. Thesis, University of Illinois at Urbana, Champaign, IL, USA, 1980.
16. Govindan, K.; Kannan, D.; Shankar, K.M. Evaluating the drivers of corporate social responsibility in the mining industry with multi-criteria approach: A multi-stakeholder perspective. *J. Clean. Prod.* **2014**, *84*, 214–232. [[CrossRef](#)]
17. Broughton, P.L. Economic geology of southern Saskatchewan potash mines. *Ore Geol. Rev.* **2019**, *113*, 103117. [[CrossRef](#)]
18. Arndt, N.T.; Fontboté, L.; Hedenquist, J.; Kesler, S.E.; Thompson, J.F.; Wood, D.G. Future global mineral resources. *Geochem. Perspect.* **2017**, *6*, 1–171. [[CrossRef](#)]
19. Kesler, S.E.; Simon, A.C.; Simon, A.F. *Mineral, Resources, Economics and the Environment*; Cambridge University Press: Cambridge, UK, 2015.
20. Baryakh, A.; Fedoseev, A.; Lobanov, S. Deformations and fracture of rock strata during deep level potash mining. *Procedia Struct. Integr.* **2021**, *32*, 109–116. [[CrossRef](#)]
21. Paraskevopoulou, C.; Vlachopoulos, N.; Diederichs, M.S. Long term tunnel behaviour and support response analysis using 2D numerical modelling methods. In Proceedings of the 46th US Rock Mechanics/Geomechanics Symposium, Chicago, IL, USA, 24–27 June 2012.
22. Kovalskii, E.R.; Gromtsev, K.V. Development of the technology of stowing the developed space during mining. *J. Min. Inst.* **2022**, *254*, 202–209. [[CrossRef](#)]
23. Khayrutdinov, A.M.; Kongar-Syuryun, C.B.; Kowalik, T.; Tyulyaeva, Y.S. Stress-strain behavior control in rock mass using different-strength backfill. *Min. Inf. Anal. Bull.* **2020**, *10*, 42–55. [[CrossRef](#)]
24. Ermolovich, E.A.; Ivannikov, A.L.; Khayrutdinov, M.M.; Kongar-Syuryun, C.B.; Tyulyaeva, Y.S. Creation of a nanomodified backfill based on the waste from enrichment of water-soluble ores. *Materials* **2022**, *15*, 3689. [[CrossRef](#)]
25. Marketos, G.; Spiers, C.J.; Govers, R. Impact of rock salt creep law choice on subsidence calculations for hydrocarbon reservoirs overlain by evaporite caprocks. *J. Geophys. Res. Solid Earth* **2016**, *121*, 4249–4267. [[CrossRef](#)]
26. Whyatt, J.; Varley, F. Catastrophic failures of underground evaporite mines. In *Proceedings of the 27th International Conference on Ground Control in Mining, Morgantown, WV, USA, 29–31 July 2008*; College of Engineering and Mineral Resources, West Virginia University: Morgantown, WV, USA, 2008; Volume 2008, p. 113.
27. King, M. Creep in model pillars of saskatchewan potash. *Int. J. Rock Mech. Min. Sci. Géoméch. Abstr.* **1973**, *10*, 363–371. [[CrossRef](#)]
28. Rybak, J.; Khayrutdinov, M.M.; Kuziev, D.A.; Kongar-Syuryun, C.B.; Babyr, N.V. Prediction of the geomechanical state of the rock mass when mining salt deposits with stowing. *J. Min. Inst.* **2022**, *253*, 61–70. [[CrossRef](#)]
29. Migliazza, M.; Chiorboli, M.; Giani, G. Comparison of analytical method, 3D finite element model with experimental subsidence measurements resulting from the extension of the Milan underground. *Comput. Geotech.* **2009**, *36*, 113–124. [[CrossRef](#)]
30. Parmar, H.; Bafghi, A.Y.; Najafi, M. Impact of ground surface subsidence due to underground mining on surface infrastructure: The case of the Anomaly No. 12 Sechahun, Iran. *Environ. Earth Sci.* **2019**, *78*, 409. [[CrossRef](#)]
31. Xu, N.; Kulatilake, P.H.; Tian, H.; Wu, X.; Nan, Y.; Wei, T. Surface subsidence prediction for the WUTONG mine using a 3-D finite difference method. *Comput. Geotech.* **2013**, *48*, 134–145. [[CrossRef](#)]
32. Vlachopoulos, N. *Back Analysis of a Tunnelling Case Study in Weak Rock of the Alpine System in Northern Greece: Validation and Optimization of Design Analysis Based on Ground Characterization and Numerical Simulation*; Library and Archives Canada: Ottawa, ON, Canada, 2011.
33. Diederichs, M.S. The 2003 Canadian Geotechnical Colloquium: Mechanistic interpretation and practical application of damage and spalling prediction criteria for deep tunnelling. *Can. Geotech. J.* **2007**, *44*, 1082–1116. [[CrossRef](#)]
34. Asadi, A.; Shahriar, K.; Goshtasbi, K.; Najm, K. Development of a new mathematical model for prediction of surface subsidence due to inclined coal-seam mining. *J. South. Afr. Inst. Min. Metall.* **2005**, *105*, 15–20.
35. Donnelly, L.; De La Cruz, H.; Asmar, I.; Zapata, O.; Perez, J. The monitoring and prediction of mining subsidence in the Amaga, Angelopolis, Venecia and Bolombolo Regions, Antioquia, Colombia. *Eng. Geol.* **2001**, *59*, 103–114. [[CrossRef](#)]
36. Sheorey, P.; Loui, J.; Singh, K.; Singh, S. Ground subsidence observations and a modified influence function method for complete subsidence prediction. *Int. J. Rock Mech. Min. Sci.* **2000**, *37*, 801–818. [[CrossRef](#)]
37. Scott, D.; Anumba, C.J. A knowledge-based system for the engineering management of subsidence cases. *Struct. Eng.* **1999**, *77*, 3.
38. Peng, S.S. *Surface Subsidence Engineering*; Society for Mining, Metallurgy, and Exploration, Inc.: Littleton, CO, USA, 1992.
39. Bahuguna, P.; Srivastava, A.; Saxena, N. A critical review of mine subsidence prediction methods. *Int. J. Min. Sci. Technol.* **1991**, *13*, 369–382. [[CrossRef](#)]

40. Sanmiquel, L.; Bascompta, M.; Vintró, C.; Yubero, T. Subsidence management system for underground mining. *Minerals* **2018**, *8*, 243. [[CrossRef](#)]
41. Carnec, C.; Delacourt, C. Three years of mining subsidence monitored by SAR interferometry, near Gardanne, France. *J. Appl. Geophys.* **2000**, *43*, 43–54. [[CrossRef](#)]
42. Zhang, A.; Lu, J.; Kim, J.-W. Detecting mining-induced ground deformation and associated hazards using spaceborne InSAR techniques. *Geomat. Nat. Hazards Risk* **2017**, *9*, 211–223. [[CrossRef](#)]
43. Modeste, G.; Doubre, C.; Masson, F. Time evolution of mining-related residual subsidence monitored over a 24-year period using InSAR in southern Alsace, France. *Int. J. Appl. Earth Obs. Geoinf.* **2021**, *102*, 102392. [[CrossRef](#)]
44. Choi, J.-K.; Won, J.-S.; Lee, S.; Kim, S.-W.; Kim, K.-D.; Jung, H.-S. Integration of a subsidence model and SAR interferometry for a coal mine subsidence hazard map in Taebaek, Korea. *Int. J. Remote Sens.* **2011**, *32*, 8161–8181. [[CrossRef](#)]
45. Herrera, G.; Fernández, M.; Tomás, R.; González-Nicieza, C.; López-Sánchez, J.; Vigil, A. Forensic analysis of buildings affected by mining subsidence based on Differential Interferometry (Part III). *Eng. Fail. Anal.* **2012**, *24*, 67–76. [[CrossRef](#)]
46. Samsonov, S.; Baryakh, A. Estimation of deformation intensity above a flooded potash mine near Berezniki (Perm Krai, Russia) with SAR interferometry. *Remote Sens.* **2020**, *12*, 3215. [[CrossRef](#)]
47. Yang, L.; Qiu, J.; Jiang, H.; Hu, S.; Li, H.; Li, S. Use of cemented super-fine unclassified tailings backfill for control of subsidence. *Minerals* **2017**, *7*, 216. [[CrossRef](#)]
48. Lee, S.; Park, I. Application of decision tree model for the ground subsidence hazard mapping near abandoned underground coal mines. *J. Environ. Manag.* **2013**, *127*, 166–176. [[CrossRef](#)]
49. Bell, F.G.; Stacey, T.R.; Genske, D.D. Mining subsidence and its effect on the environment: Some differing examples. *Environ. Earth Sci.* **2000**, *40*, 135–152. [[CrossRef](#)]
50. Rateb, A.; Abotalib, A.Z. Inferencing the land subsidence in the Nile Delta using Sentinel-1 satellites and GPS between 2015 and 2019. *Sci. Total Environ.* **2020**, *729*, 138868. [[CrossRef](#)]
51. Bitelli, G.; Bonsignore, F.; Del Conte, S.; Novali, F.; Pellegrino, I.; Vittuari, L. Integrated use of advanced InSAR and GPS data for subsidence monitoring. In *Engineering Geology for Society and Territory-Volume 5*; Lollino, G., Manconi, A., Guzzetti, F., Culshaw, M., Bobrowsky, P., Luino, F., Eds.; Springer: Cham, Switzerland, 2015; pp. 147–150.
52. Bürgmann, R.; Hilley, G.; Ferretti, A.; Novali, F. Resolving vertical tectonics in the San Francisco Bay Area from permanent scatterer InSAR and GPS analysis. *Geology* **2006**, *34*, 221. [[CrossRef](#)]
53. de Orellana, A.C. Pressure solution creep and non-associated plasticity in the mechanical behavior of potash mine openings. *Int. J. Rock Mech. Min. Sci. Géoméch. Abstr.* **1996**, *33*, 347–370. [[CrossRef](#)]
54. Cendón, D.; Ayora, C.; Pueyo, J.; Taberner, C. The geochemical evolution of the Catalan potash subbasin, South Pyrenean foreland basin (Spain). *Chem. Geol.* **2003**, *200*, 339–357. [[CrossRef](#)]